AMERICAN SOCIETY FOR MICROBIOLOGY | Antimicrobial Agents and Chemotherapy®

PHARMACOLOGY

Population Pharmacokinetic Modeling as a Tool To Characterize the Decrease in Ciprofloxacin Free Interstitial Levels Caused by *Pseudomonas aeruginosa* Biofilm Lung Infection in Wistar Rats

Bruna G. S. Torres,[a] Victória E. Helfer,[a] Priscila M. Bernardes,[a] Alexandre José Macedo,[a,b] Elisabet I. Nielsen,[c] Lena E. Friberg,[c] Teresa Dalla Costa[a]

Pharmaceutical Sciences Graduate Program, College of Pharmacy, Federal University of Rio Grande do Sul, Porto Alegre, Brazil[a]; Centro de Biotecnologia, Federal University of Rio Grande do Sul, Porto Alegre, Brazil[b]; Department of Pharmaceutical Biosciences, Uppsala University, Uppsala, Sweden[c]

ABSTRACT Biofilm formation plays an important role in the persistence of pulmonary infections, for example, in cystic fibrosis patients. So far, little is known about the antimicrobial lung disposition in biofilm-associated pneumonia. This study aimed to evaluate, by microdialysis, ciprofloxacin (CIP) penetration into the lungs of healthy and *Pseudomonas aeruginosa* biofilm-infected rats and to develop a comprehensive model to describe the CIP disposition under both conditions. *P. aeruginosa* was immobilized into alginate beads and intratracheally inoculated 14 days before CIP administration (20 mg/kg of body weight). Plasma and microdialysate were sampled from different animal groups, and the observations were evaluated by noncompartmental analysis (NCA) and population pharmacokinetic (popPK) analysis. The final model that successfully described all data consisted of an arterial and a venous central compartment and two peripheral distribution compartments, and the disposition in the lung was modeled as a two-compartment model structure linked to the venous compartment. Plasma clearance was approximately 32% lower in infected animals, leading to a significantly higher level of plasma CIP exposure (area under the concentration-time curve from time zero to infinity, 27.3 ± 12.1 μg · h/ml and 13.3 ± 3.5 μg · h/ml in infected and healthy rats, respectively). Despite the plasma exposure, infected animals showed a four times lower tissue concentration/plasma concentration ratio (lung penetration factor = 0.44 and 1.69 in infected and healthy rats, respectively), and lung clearance (CL_{lung}) was added to the model for these animals (CL_{lung} = 0.643 liters/h/kg) to explain the lower tissue concentrations. Our results indicate that *P. aeruginosa* biofilm infection reduces the CIP free interstitial lung concentrations and increases plasma exposure, suggesting that plasma concentrations alone are not a good surrogate of lung concentrations.

KEYWORDS biofilm, *Pseudomonas aeruginosa*, ciprofloxacin, microdialysis, pneumonia, population pharmacokinetics

Received 1 December 2016 **Returned for modification** 29 January 2017 **Accepted** 9 April 2017

Accepted manuscript posted online 1 May 2017

Citation Torres BGS, Helfer VE, Bernardes PM, Macedo AJ, Nielsen EI, Friberg LE, Dalla Costa T. 2017. Population pharmacokinetic modeling as a tool to characterize the decrease in ciprofloxacin free interstitial levels caused by *Pseudomonas aeruginosa* biofilm lung infection in Wistar rats. Antimicrob Agents Chemother 61:e02553-16. https://doi.org/10.1128/AAC.02553-16.

Address correspondence to Teresa Dalla Costa, dalla.costa@ufrgs.br.

Chronic respiratory infection (CRI) is characterized by progressive cycles of infection and inflammation culminating in respiratory failure (1). Biofilm formation is the main cause of the CRI persistence since it provides increased resistance to antibiotics and to host defense. The immune system and the antibacterial therapy can no longer eradicate the bacteria, and patients have an accelerated decline in pulmonary function that leads to a poor prognosis and increased mortality (2).

CRI is the primary cause of morbidity and mortality in cystic fibrosis (CF) patients (3),

and *Pseudomonas aeruginosa* is the pathogen isolated from the lungs of about 80% of adults with CF (1, 4). Ciprofloxacin (CIP) is regarded as an antipseudomonal fluoroquinolone since it shows high antimicrobial potency against *P. aeruginosa* (5) and is used both in the prevention and in the treatment of *P. aeruginosa* CRI in CF patients.

The treatment of biofilm infections is a clinical challenge, and the establishment of an efficient dosing regimen is important to maximize the effects of antimicrobials and to prevent the development of resistance (6). Antimicrobial dosing regimen optimization is traditionally based on pharmacokinetic (PK) and pharmacodynamic (PD) information obtained from studies with planktonic bacteria. Only a few studies of PK and PD with biofilm bacteria have been reported (6–8). Therefore, increasing the knowledge of the disposition (PK) of antimicrobial agents in biofilm infections can contribute to improve the clinical outcome of biofilm-associated diseases.

Most of the PK/PD studies with antimicrobial agents use free plasma levels of the drug to evaluate the dosing regimen and to predict efficacy, assuming that free plasma levels are a good surrogate for free concentrations in the infected tissue. This assumption has been challenged by microdialysis studies of unbound antimicrobial tissue concentrations showing that discrepancies between free plasma and free tissue concentrations may occur in tissues with active transporters, where efflux and influx processes can contribute to the drug distribution (9, 10). Additionally, pathological conditions can change tissue-blood relationships, and antimicrobial concentrations in infected tissues may differ from those in healthy tissues due to increased temperature, decreased pH, plasma extravasation, and leukocyte migration at the infection site (11).

Studies conducted with bacteria in the planktonic form showed that pneumonia may affect or not affect the lung penetration of antimicrobials (12–15). While for imipenem no differences in the distribution in the extracellular fluid (ECF) of the lung were found for healthy and *Acinetobacter baumannii*-infected rats (12, 13), for tigecycline the presence of *Acinetobacter baumannii* in mouse lungs enhanced the penetration of the drug into the epithelial lining fluid (ELF) (14). After Monte Carlo simulations, Kuti and Nicolau (15) showed that the simulated levofloxacin exposure in ELF was lower for infected patients than for noninfected patients. Whether pulmonary infection with biofilm formation can alter antimicrobial lung penetration has not been demonstrated. The present study was conducted to evaluate, by microdialysis, CIP free concentrations in the lung interstitial fluid of healthy and *P. aeruginosa* biofilm-infected Wistar rats and to develop a population pharmacokinetic (popPK) model that adequately describes the rate and extent of pulmonary penetration and the correlation between plasma and lung concentrations in both situations. A popPK model that simultaneously fits total plasma and free tissue concentrations has the potential to increase knowledge about the antimicrobial lung distribution and serve as a useful tool to establish a more efficient dosing regimen for biofilm-associated infections.

RESULTS

Rat model of biofilm lung infection. The beads containing *P. aeruginosa* cells used for inoculation of the animals had an average size of 222 μm (range, 89 to 376 μm), and the bead population was homogeneous, as indicated by the low polydispersity of the particle sizes (span value = 1.559). The animal lung infection model was able to sustain the infection for 14 days. The histopathological analysis revealed that the lungs of infected animals showed multifocal inflammatory infiltrates composed predominantly of lymphocytes, plasma cells, macrophages, and intact and degenerated neutrophils within the bronchi and bronchioles (Fig. 1a to c). There was also moderate multifocal congestion and thickening of the alveolar septa, besides multifocal areas with emphysema, characterizing pyogranulomatous pneumonia. For the animals inoculated with the blank beads, inflammatory infiltrates in the lung were not observed, although lung congestion and diffuse areas of bleeding due to the euthanasia procedure were noted (Fig. 1d to f). The lung infection model was homogeneous, as shown in Fig. 1, in which all the animals of the same group had the same physiological changes.

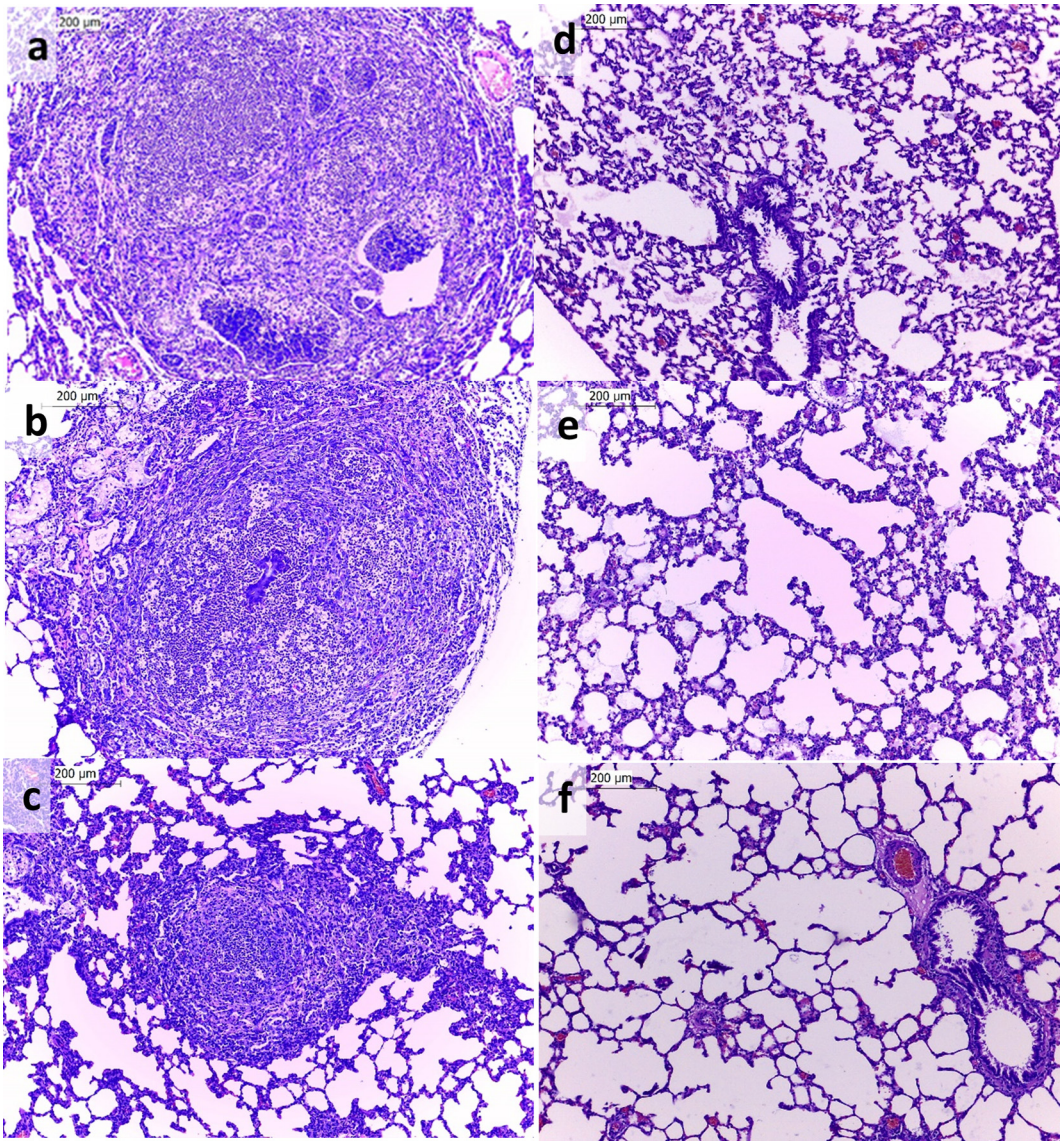

FIG 1 Photomicrographs of hematoxylin- and eosin-stained sections of lungs from infected rats (a to c) and rats inoculated with blank beads (d to f). Each photomicrograph represents a different animal ($n = 3$ animals/group). Magnifications, ×100.

The rat model of biofilm lung infection used in the CIP lung penetration study was successful in establishing a chronic infection that mimics the pulmonary infections observed in CF patients. The bead size and the time after inoculation (14 days) used in this study were chosen on the basis of the findings of previous studies (16, 17) to be more reflective of the infection seen in CF patients.

***In vitro* and *in vivo* calibration of microdialysis probes.** For the *in vitro* calibration of the microdialysis probes, the relative recoveries were determined by dialysis and retrodialysis. For flow rates of 1.0, 1.5, and 2.0 μl/min, the relative recoveries by dialysis (RR_Ds) were 29.7% ± 2.9%, 23.0% ± 2.8%, and 15.4% ± 3.1%, respectively, and the relative recoveries by retrodialysis (RR_{RD}s) were 31.6% ± 2.9%, 22.8% ± 1.6%, and 15.4% ± 3.1%, respectively. For the same flow rates, the relative recoveries determined by dialysis and retrodialysis were statistically significantly similar ($\alpha = 0.05$), indicating that CIP does not bind to microdialysis tubing and that retrodialysis can be used to determine the relative recovery *in vivo*. As expected, as the perfusate flow rate increased, the relative recovery decreased. The 1.5 μl/min flow rate was chosen as the work flow for the *in vivo* experiments because it allows the collection over a short

TABLE 1 CIP pharmacokinetic parameters determined by NCA in plasma and lung after 20 mg/kg i.v. bolus dosing to healthy, *P. aeruginosa* biofilm-infected, and blank bead-inoculated Wistar rats[c]

	Plasma		Lung microdialysis		
PK parameter	Healthy rats	Infected rats	Healthy rats	Infected rats	Blank bead-inoculated rats
$t_{1/2}$ (h)	3.1 ± 0.8	5.9 ± 2.7[a]	3.0 ± 0.4	3.3 ± 0.8	3.3 ± 0.7
AUC_{0-12} (μg · h/ml)	12.4 ± 2.7	19.8 ± 5.9	15.1 ± 6.3	7.9 ± 1.5	13.8 ± 5.1
$AUC_{0-\infty}$ (μg · h/ml)	13.3 ± 3.5	27.3 ± 12.1[a]	15.8 ± 6.6	8.4 ± 1.8[b]	15.2 ± 5.9
MRT (h)	3.4 ± 1.2	7.8 ± 3.9[a]			
CL (liters/h/kg)	1.59 ± 0.41	0.89 ± 0.44[a]			
V (liters/kg)	5.08 ± 0.68	5.61 ± 1.08			
fT			1.69	0.44	1.63

[a]Statistically significant difference compared to the healthy group based on Student's *t* test ($\alpha = 0.05$).
[b]Statistically significant difference compared to the healthy and blank bead-inoculated groups based on one-way ANOVA with Tukey's test (pos hoc) ($\alpha = 0.05$).
[c]Data represent averages ± standard deviations ($n = 6$ rats/group). For microdialysis data, the midpoint approach was utilized in all calculations. Abbreviations: $t_{1/2}$, elimination half-life; AUC_{0-12}, area under the concentration-time curve from time zero to 12 h; $AUC_{0-\infty}$, area under the concentration-time curve from time zero to infinity; MRT, mean residence time; CL, total clearance; *V*, volume of distribution; *fT*, lung penetration factor ($AUC_{0-\infty,tissue,\ free}/f_u \cdot AUC_{0-\infty,plasma}$, where the plasma f_u is equal to 0.70).

period of time (30 min), in relation to the CIP half-life, of sample volumes that are large enough.

The influence of CIP concentrations on the microdialysis probe recoveries was evaluated by both methods using the 1.5 μl/min flow rate. The average RR_Ds determined were 22.1% ± 1.7%, 24.3% ± 3.7%, and 23.1% ± 2.8% for CIP concentrations of 0.25, 0.75, and 1.5 μg/ml, respectively. For the retrodialysis method, the RR_{RD}s were 21.0% ± 1.8%, 24.8% ± 4.4%, and 24.7% ± 5.2% for the same concentrations, respectively. No statistically significant differences ($\alpha = 0.05$) in the values obtained between the methods (dialysis and retrodialysis) or between the CIP concentrations tested (0.25, 0.75, and 1.5 μg/ml) were observed, indicating that the relative recovery of the probes is concentration independent.

The *in vivo* recovery was determined by retrodialysis using the 1.5 μl/min flow rate chosen. No differences in the *in vivo* lung relative recovery were observed between healthy animals (11.3% ± 1.9%) and infected animals (12.2% ± 0.5%). The *in vivo* RR_{RD} was lower than the recovery rate determined *in vitro*, which could be explained by tissue characteristics, such as tissue protein binding, blood flow, interstitial volume, and tissue tortuosity, as previously reported for other drugs (18, 19). The *in vivo* recoveries were employed to calculate the true lung free levels, measured by microdialysis, in healthy and infected animals.

Plasma protein binding. CIP showed a low level of protein binding in rat plasma (29.8% ± 5.9%) independently of the drug concentration over the concentration range investigated (0.3 to 6 μg/ml). The average unbound (free) fraction (f_u) of 0.70 was used in the popPK model for prediction of free plasma levels on the basis of the total plasma concentrations and in the noncompartmental analysis (NCA) for the calculation of the free plasma area under the concentration-time curve (AUC) from time zero to infinity ($f_u \cdot AUC_{0-\infty,plasma}$) to determine the CIP lung penetration factor (*fT*).

Noncompartmental analysis. The parameters obtained by NCA of total plasma and microdialysis data following intravenous (i.v.) dosing of CIP at 20 mg/kg of body weight (BW) are summarized in Table 1. The CIP dose used in this study (20 mg/kg) was chosen on the basis of the dose used to treat pneumonias in CF patients. The dose was adjusted for animals using allometric scaling (20), based on the basal metabolic rate of rats and adults.

For healthy and infected rats, statistically significant differences in the plasma clearance (CL; 1.59 ± 0.41 liters/h/kg and 0.89 ± 0.44 liters/h/kg, respectively) and the elimination rate constant (0.23 ± 0.04 h^{-1} and 0.14 ± 0.08 h^{-1}, respectively) were observed. No statistically significant differences in the volume of distribution at steady state (V_{SS}) were observed between healthy and infected rats (5.08 ± 0.68 liters/kg and 5.61 ± 1.08 liters/kg, respectively). The free interstitial pulmonary penetration observed in infected rats ($fT = 0.44$) was four times lower than that observed in healthy animals

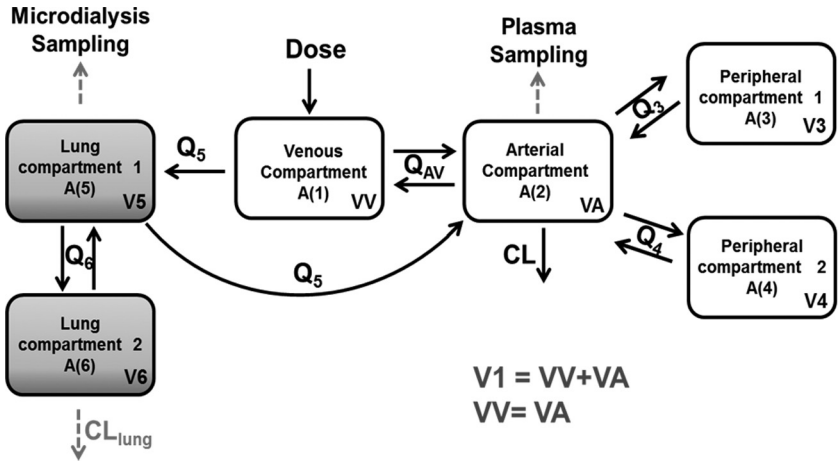

FIG 2 Schematic representation of the final CIP lung and plasma model. Abbreviations: A (1), amount of drug in the venous compartment; A (2), amount of drug in the arterial compartment; A (3) and A (4), amount of drug in the two peripheral compartments; A (5) and A (6), amount of drug in the two lung compartments; Q_{AV}, intercompartmental clearance in the blood; Q_3, Q_4, Q_5, and Q_6, intercompartmental clearances; VV, volume of the venous compartment; VA, volume of the arterial compartment; V3 and V4, volumes of the two peripheral compartments; V5 and V6, volumes of the two lung compartments; CL, central clearance; CL_{lung}, lung clearance.

($fT = 1.69$), with no significant differences in the lung elimination rate constants being observed between healthy animals ($\lambda = 0.23\ h^{-1} \pm 0.03\ h^{-1}$) and infected animals ($0.22 \pm 0.06\ h^{-1}$) rats. The infected animals showed a higher variability (higher standard deviations) in all plasma PK parameters investigated. All PK parameters determined for the blank bead-inoculated group were similar to those determined for the healthy group, with no difference in the free interstitial pulmonary penetration being detected ($fT = 1.63$).

Population pharmacokinetic modeling. Plasma data were best fitted to a three-compartment open model with first-order elimination. When the model was expanded to include unbound lung data, the central compartment was separated into arterial and venous compartments to explain the high initial free CIP levels observed in the lungs. Administration was set to occur in the venous compartment, since CIP was administered into the femoral vein, and plasma sampling was assumed to be from the arterial compartment because blood was collected from the carotid artery. The final model consisted of an arterial compartment and a venous compartment, two compartments representing different regions of the lungs, and two peripheral distribution compartments, representing tissues other than lungs (Fig. 2). The intercompartmental clearance between the venous and arterial compartments (intercompartmental clearance in the blood [Q_{AV}] = 4.4 liters/h/kg) was fixed to the reported value of cardiac output in urethane-anesthetized rats (21). Drug elimination was assumed to occur from the arterial compartment. The final model had interindividual variability on clearance (CL), intercompartmental clearance for the first peripheral compartment (Q_3), and the volumes of both lung compartments (V5 and V6). All parameters were allometrically scaled with the individual rat body weights. Residual variability was described by a proportional error for plasma data and combined (proportional plus additive) error for microdialysis data. A significant infection effect ($P < 0.01$) was detected for CL, lung intercompartmental clearance (Q_6), and lung volume (V6), and in the final model, these parameters were estimated separately for the infected animals (CL_{INFEC}, $Q_{6\ INFEC}$, and $V6_{INFEC}$, respectively). A reduction in the plasma clearance for the infected animals (CL_{INFEC}) of approximately 32% was observed. Additionally, an almost 200% increase in the lung intercompartmental clearance ($Q_{6\ INFEC}$) and a 511% increase in the lung volume ($V6_{INFEC}$) were observed in infected animals. No significant bead effect was observed for any parameter. Drug elimination from the lungs (lung clearance [CL_{lung}]) was added to the model for microdialysis data from infected animals to explain the

TABLE 2 Parameter estimates of the final CIP model[a]

Model and parameter	Estimate (% RSE)	Median SIR (95% CI)	% CV for IIV (%RSE)	% shrinkage
Structural model				
CL (liters/h/kg)	0.615 (5)	0.618 (0.562–0.686)	31.7 (11)[b]	−0.79
CL_{INFEC} (liters/h/kg)	0.416 (12)	0.418 (0.323–0.524)		
V1 (liters/kg)	0.0232 (15)	0.0237 (0.0173–0.0305)		
Q_{AV} (liters/h/kg)	4.4 FIX			
Q_3 (liters/h/kg)	0.174 (17)	0.173 (0.129–0.245)	77.6 (12)	6.33
V3 (liters/kg)	1.433 (6)	1.429 (1.291–1.595)		
Q_4 (liters/h/kg)	0.352 (15)	0.355 (0.253–0.463)		
V4 (liters/kg)	0.474 (11)	0.476 (0.368–0.577)		
Q_5 (liters/h/kg)	0.381 (19)	0.389 (0.273–0.550)		
V5 (liters/kg)	0.291 (16)	0.295 (0.202–0.391)	83.7 (12)	6.23
Q_6 (liters/h/kg)	0.269 (17)	0.273 (0.201–0.380)		
$Q_{6\ INFEC}$ (liters/h/kg)	0.529 (18)	0.528 (0.354–0.731)		
V6 (liters/kg)	0.187 (19)	0.188 (0.121–0.265)	78.9 (17)[b]	9.76
$V6_{INFEC}$ (liters/kg)	0.957 (29)	1.01 (0.516–1.55)		
CL_{lung} (liters/h/kg)	0.643 (19)	0.660 (0.427–0.921)		
Residual variability				
Plasma proportional error (%)	6.83 (10)	6.86 (5.79–8.38)		
Microdialysis proportional error (%)	9.10 (5)	9.12 (8.28–10.10)		
Microdialysis additive error (mg/liter)	0.014 (15)	0.014 (0.0098–0.017)		
Shrinkage IWRES (%)	10.08			

[a]Abbreviations: CL, clearance; *Q*, intercompartmental clearance; *V*, volume; RSE, relative standard error; CI, confidence interval; SIR, sampling importance resampling; IIV, interindividual variability; CV, coefficient of variation. FIX, fixed value; IWRES, individual weighted residuals. All parameters are scaled on the basis of rat body weight.

[b]Interindividual variability was shared between both parameters.

discrepancy observed between lung and plasma exposure. The inclusion of this extra parameter led to a drop in the objective function value (OFV) of 59.1 points and a better fit of the model to the data for the infected groups. Additionally, the value estimated for this lung clearance (CL_{lung} = 0.643 liter/h/kg) was approximately of the same magnitude as the central clearance (CL = 0.615 liter/h/kg), showing the importance of this extra parameter for infected animals. Our model and data suggest that differences in other physiological processes besides only differences in distribution occur in the infected animals, given that parameters that describe the changes in the CIP distribution ($Q_{6\ INFEC}$ and $V6_{INFEC}$) and parameters other than distribution (CL_{lung}) are necessary to describe the infected-animals data.

All parameters of the final PK model were well estimated with low relative standard errors (Table 2). The individual and population model predictions provided a good fit to the plasma and lung data for all groups (healthy and infected rats and blank bead-inoculated rats) (Fig. 3). The final PK model estimates were used to simulated 5,000 concentrations-time profiles, and the visual predictive checks (VPCs) resulting from these simulations were stratified by plasma or lung concentrations and by the 3 different groups (healthy and infected animals and blank bead-inoculated animals) and are shown in Fig. 4. The VPCs confirmed that the model adequately predicts both the plasma and lung concentration data. For the healthy group, a slight overprediction of the terminal phase for plasma data and an underprediction of the initial time points for microdialysis data could be observed in the VPC simulations. These slight over- and underpredictions probably occurred because of the small number of individuals per group (n = 6 animals/group), where a greater influence of the value for one individual on the median is expected.

DISCUSSION

In the present study, free CIP lung concentrations were evaluated in healthy and *P. aeruginosa* biofilm-infected Wistar rats using microdialysis. Given that in many cases plasma concentrations may not reflect tissue concentrations (9, 18, 22) and infection may (22) or may not (13) alter the antimicrobial tissue disposition, knowledge of the antimicrobial pharmacologically active free interstitial concentrations is crucial to better

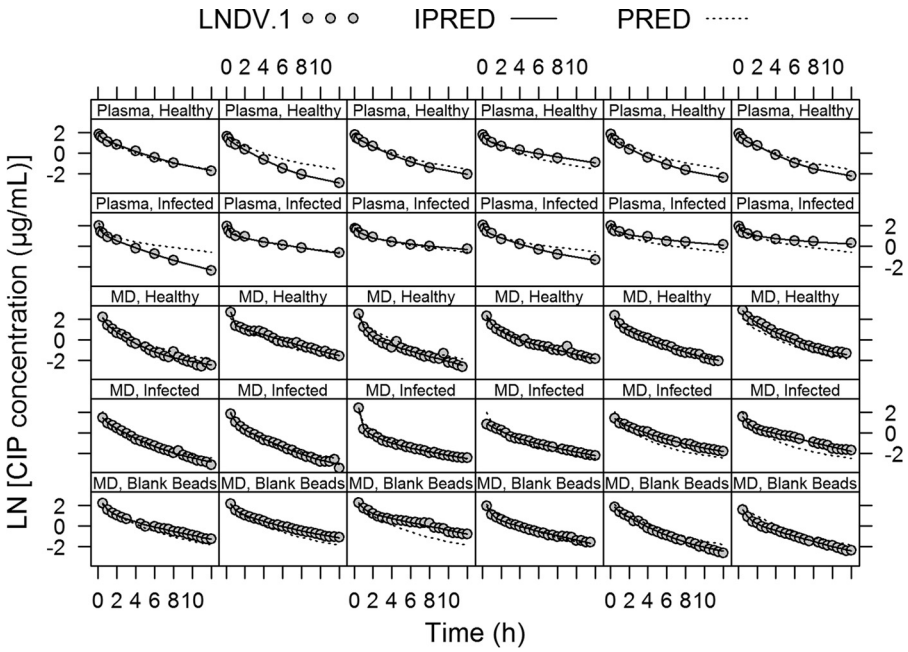

FIG 3 Individual and population fitted plasma and microdialysis (MD) concentration-versus-time profiles using the final popPK model. Gray dots, observations (LNDV.1); solid lines, individual model predictions (IPRED); dashed lines, population model predictions (PRED).

design dosing regimens (23). Our results showed discrepancies between the free plasma and free interstitial lung concentrations in the rat model of biofilm infection, which mimics the pulmonary infection observed in CF patients. *Pseudomonas aeruginosa* biofilm-infected rats showed higher plasma exposure, although lower free CIP levels were founded in the interstitial lung fluid of infected animals than in that of healthy animals.

The group inoculated with blank alginate beads, without *P. aeruginosa*, was used to determine whether the eventual differences observed in the lung pharmacokinetic parameters of the infected animals were due to the presence of the biofilm-forming bacteria or were an artifact of the beads used for inoculation. No significant effect of the beads could be observed in the CIP pharmacokinetic parameters (Table 1), and the data for the blank beads were well fitted (Fig. 4) with the same parameters used to fit the data from the healthy animals, indicating that alginate beads do not produce alterations in the lung that could influence CIP penetration. These results are also in

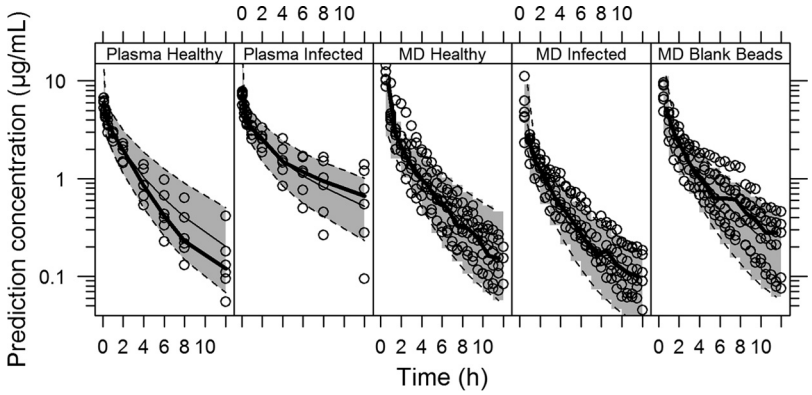

FIG 4 Visual predictive checks (VPCs) of the final population PK model stratified by compartment (plasma or lung) and group (healthy or infected rats or blank bead-inoculated rats). VPCs are based on 5,000 simulations and show a comparison of the observations (dots and thick lines for the median) with the 10th and 90th percentiles of the 5,000 simulated profiles (dashed lines and shaded areas).

accordance with those of the histopathological analysis that indicated that no inflammation was present in the lungs of animals inoculated with blank beads 14 days after bead inoculation.

A simultaneous pharmacokinetic modeling of total plasma and free lung CIP concentrations allowed for quantification of the rate and extent of the lung distribution and the plasma and lung data in healthy and biofilm-infected rats. The central compartment was divided into venous and arterial compartments to characterize the high early free CIP levels achieved in the lung compared to arterial plasma. Given that CIP was administered intravenously and plasma was sampled from the carotid artery, the higher lung levels can be explained by the pulmonary circulation, where venous blood leaves the heart, enters the lungs, and returns oxygenated (arterial blood) back to the heart (24). In the model, the lung compartment is connected to the venous compartment and returns to the arterial compartment (Fig. 2), as suggested previously in physiologically based pharmacokinetic models (24–26). Initially, lung data were modeled as a single compartment, but this approach resulted in a poor fit. When the lung was divided into two compartments, the OFV dropped more than 100 points and a significant improvement in the model fit was observed. Due to the fact that lungs have a complex anatomy with different tissue structures and the complex anatomy can prevent the uniform distribution of drugs, the two lung compartments represent the parts of the lung in which CIP can have different affinities and distribution properties. Microdialysis measurements were assumed to take place in the first compartment; therefore, this compartment includes the pulmonary interstitial fluid (Fig. 2).

The NCA results showed that *P. aeruginosa* biofilm infection could affect an animal's exposure to CIP. The significantly higher CIP plasma exposure in infected animals (area under the concentration-time curve from time zero to infinity [$AUC_{0-\infty}$] = 27.3 ± 12.1 μg · h/ml) than in healthy animals ($AUC_{0-\infty}$ = 13.3 ± 3.5 μg · h/ml) can be explained by the significant 32% reduction in clearance from the central compartment observed in infected animals (α = 0.05). In the stepwise covariate modeling (SCM) analysis, the inclusion of infection as a covariate for clearance was statistically significant. It has been reported earlier that infectious or inflammatory disease states can modulate drug pharmacokinetics via different mechanisms (27). Infections and inflammatory states may alter the rate of blood flow to the liver and kidney, major organs for drug clearance, with a consequent decrease in elimination rates. Moreover, studies have demonstrated that infection and inflammation are associated with the downregulation of hepatic and extrahepatic cytochrome P450s, and alterations of PK parameters, such as decreased clearance, have been observed for humans and animals infected with Gram-positive and Gram-negative bacteria (27). Since CIP is eliminated by a combination of nonrenal and renal excretion (28, 29), the changes in the liver and kidneys induced due to both infection and inflammation may explain the higher CIP plasma exposure observed in the infected animals.

A high level of CIP lung penetration in healthy animals was observed using microdialysis (fT = 1.69). High levels of lung penetration have been shown earlier for CIP and other fluoroquinolones in microdialysis studies (10), from epithelial lining fluid (ELF) measurements (30), and from tissue homogenate measurements (31, 32) for both humans and rats. A penetration factor higher than 1 ($fT > 1$) indicates that transporters and/or ion trapping can be involved in the CIP distribution to the lung, as previously shown for levofloxacin (10). CIP interstitial lung exposure in animals infected with biofilm-forming bacteria ($AUC_{0-\infty}$ = 8.4 ± 1.8 μg · h/ml) was approximately half of that in healthy animals ($AUC_{0-\infty}$ = 15.8 ± 6.6 μg · h/ml), indicating that the chronic inflammation resulting from pneumonia causes physiological alterations in the lung, leading to a decrease in free interstitial drug concentrations. Although the NCA results for microdialysis data should be interpreted with caution, since it is the average concentration during the interval which is assayed and interpolation from time zero to the midpoint of the initial time interval may result, in that a relatively large proportion of the AUC may be missed, the covariate analysis in the PK modeling also revealed that the lung distribution was significantly affected by the infection. A two times higher

intercompartmental clearance between the two lung compartments (Q_6) and a five times higher volume of the second lung compartment (V6) were observed in the infected than in the healthy ones (Table 2). These changes result in an increased CIP distribution to the second lung compartment, since the increase in Q_6 without changes in the volume of the first compartment (V5) leads to an increase in the distribution rate microconstant ($k_{56} = Q_6/V5$), which describes the distribution from the first to the second lung compartment. Additionally, a decrease in the opposite distribution rate microconstant ($k_{65} = Q_6/V6$) was also observed due to a higher increase in V6 than in Q_6. The results thereby indicate that a larger amount of the drug stayed in the second lung compartment of the infected animals, decreasing CIP levels in the first compartment, where we assume that the microdialysis probe was placed, resulting in lower concentrations available to be sampled.

Despite having a higher total plasma exposure and, consequently, more drug that could distribute into the tissues, the infected animals presented the lowest levels of lung interstitial fluid exposure ($AUC_{0-\infty} = 8.4 \pm 1.8$ μg · h/ml; Table 1), resulting in a lower lung penetration factor (fT = 0.44). An extra parameter, drug elimination from the lungs (CL_{lung}), was added to the model for the microdialysis probe-infected animals to explain this discrepancy. Local lung changes due to infection/inflammation can alter the local drug distribution without interfering with systemic exposure, requiring a specific extra parameter to describe the changes observed in this biophase.

These differences in PK parameters observed in the lungs of infected animals may have been due to the physiological changes that occur in infected and inflamed tissues, such as increases in vascular permeability and the tissue temperature and alterations of tissue pH (11). Studies conducted in healthy animals showed that the concentration of protein in ELF is much lower than that in serum (33), and the level of binding to ELF proteins can be considered negligible for drugs with a low level of protein binding, such as CIP. However, during bacterial infection, the inflammation and tissue damage result in increased vascular permeability and a higher protein content in ELF (34). Additionally, infection promotes the migration of white blood cells to the site of infection, increasing the cellular mass locally (34). The higher cellular mass at the site of active infection can increase the intracellular amount of antimicrobials, such as fluoroquinolones, which penetrate intracellularly. Furthermore, changes in the tissue pH due to infection may alter the ion-trapping characteristics of CIP, an amphoteric drug, and more drug can be ionized intracellularly and not be able to diffuse back to the interstitial fluid. One cannot discharge the hypothesis that the lower CIP concentrations in infected lung interstitial fluid could be in part due to the presence of a biofilm matrix. Experimental data from *in vitro* studies have shown that some antimicrobials can interact with the biofilm matrix (35). It has been shown that CIP can easily penetrate the *P. aeruginosa* biofilm matrix (36), and fluoroquinolones show high levels of permeation of *P. aeruginosa* alginate (37).

Together, the physiological alterations that take place in the infected lung can support the results found in pneumonic rats. Because CIP concentrations were measured only in the interstitial fluid and no measurements were made in other regions of the lung, such as ELF or intracellularly, the lower levels of CIP observed in infected animals may be due to a reduced availability of free drug in the interstitial fluid captured by the microdialysis probe. CL_{lung} represents the process in which CIP stays entrapped in the lung and is not able to redistribute (ion trapping, with CIP being retained inside the biofilm), and the differences in Q_6 and V6 represent changes in the CIP distribution process (increase in protein content and cellular mass). Distribution changes due to infection may occur in both lung compartments, although our data and model suggest that the physiological changes caused by the infection were more relevant in the second compartment. Thereby, we assume that the changes that occur in the lung tissue—the increase in the protein concentration, the increase in the numbers of macrophages, increased amounts of mucus, and the biofilm matrix—were more significant for the second compartment.

In summary, a population PK model was successfully developed to simultaneously

characterize CIP total plasma and free lung interstitial fluid concentrations in healthy and *P. aeruginosa* biofilm-infected rats. The developed model allowed us to integrate all experimental data and to adequately describe the changes in the plasma and lung distributions of CIP observed in biofilm-forming bacterial pneumonia. Our findings indicate that the use of total plasma concentrations and even free plasma concentration is inappropriate to optimize an effective CIP dosing regimen to treat lung infections caused by biofilm-forming bacteria. The results reiterate the importance of developing a predictive popPK model since determination of the free antimicrobial concentrations at the site of infection is not always feasible. In conclusion, for adequate adjustment of the CIP dose to treat biofilm-forming bacterial pneumonia, plasma concentrations may be used to predict the pharmacologically active free interstitial lung concentration using the popPK model described in this study.

MATERIALS AND METHODS

Bacterial strain, chemicals, and solutions. *Pseudomonas aeruginosa* ATCC 27853 was used in this study. Mueller-Hinton broth and agar were purchased from Fluka (St. Gallen, Switzerland). Ciprofloxacin (purity $\geq$ 98.0%), urethane (ethyl carbamate, purity $\geq$ 99.0%), and alginic acid sodium salt from brown algae (CAS 9005-38-3) were purchased from Sigma-Aldrich (St. Louis, MO, USA). Heparin (5,000 IU/ml) was purchased from Cristália Produtos Químicos Farmacêuticos (São Paulo, Brazil). Ringer's solution consisted of 147 mM NaCl, 1.3 mM $CaCl_2$, and 4 mM KCl. Sodium chloride, calcium chloride, and potassium chloride were of analytical reagent grade and purchased from commercial sources. Ciprofloxacin was prepared in saline (10 mg/ml) with the addition of a few drops of 0.1 N HCl, and the pH was adjusted to 6.0 $\pm$ 0.5 prior to administration to the animals.

Quantification of CIP in rat plasma and microdialysate samples. The quantification of CIP in plasma and microdialysate samples was performed by a validated liquid chromatography (LC) fluorescence detection method (38).

Briefly, for plasma analysis, a mixture of 0.4% aqueous triethylamine (the pH was adjusted to 3.0 $\pm$ 0.1 with 85% phosphoric acid)-acetonitrile (88:12, vol/vol) was used as mobile phase at a flow rate of 1.2 ml/min. Ten microliters of internal standard (levofloxacin at 5 μg/ml) was added to 100 μl plasma aliquots, and proteins were precipitated by the addition of 200 μl of ice-cold methanol containing 0.5% formic acid. The samples were shaken for 5 min, followed by 10 min of centrifugation at 4 $\pm$ 1°C and 12,000 rpm. Twenty microliters of the supernatant was injected into the LC system. The concentrations on the plasma standard curve ranged from 10 to 2,000 ng/ml.

For the microdialysate samples, the mobile phase consisted of a mixture of 0.4% aqueous triethylamine (the pH was adjusted to 3.0 $\pm$ 0.1 with 85% phosphoric acid)-methanol-acetonitrile (75:15:10, vol/vol/vol) at a flow rate of 1.0 ml/min. Twenty microliters of the microdialysate samples was injected directly into the system without sample processing. The concentrations on the microdialysate standard curve ranged from 5 to 1,000 ng/ml.

For both methods, a reversed-phase C_{18} column (Atlantis T3 column; 150 by 4.6 mm; particle size, 5 μm; Waters, Milford, MA, USA) coupled to a C_{18} guard cartridge (4.0 by 3.0 mm; particle size, 4 μm; Phenomenex, Torrance, CA, USA) was used. The chromatographic analysis was carried out on a Shimadzu system equipped with an LC-10AD VP pump, a SIL-10AD VP autoinjector, an SCL-10A VP system controller, and a DGU-14A degasser, and the fluorescence detector was set at excitation and emission wavelengths of 278 nm and 453 nm, respectively.

Microdialysis system. CMA/20 microdialysis probes (membrane length, 4 mm; molecular mass cutoff, 20 kDa; CMA Microdialysis, Kista, Sweden) were employed in this study. Each probe was coupled to a microliter syringe (500 μl; Hamilton Company, Reno, NV, USA) to provide the perfusion of the Ringer's solution using a PHD 2000 syringe pump (Harvard Apparatus, Holliston, MA, USA).

Microdialysis probe *in vitro* calibration. Initially, the *in vitro* microdialysis experiments were performed with the view to investigate the influence of the flow rate and CIP concentration on microdialysis probe relative recovery (RR). The influences of the perfusion flow rate and concentration were investigated using dialysis and retrodialysis methods (18).

For the dialysis method, the microdialysis probes ($n = 3$) were placed in a glass tube containing CIP at different concentrations in Ringer's solution. Blank Ringer's solution was pumped through the probes, and microdialysate samples were collected and analyzed by the LC fluorescence detection method. The relative recovery by dialysis (RR_D; in percent) was calculated according to equation 1:

$$RR_D = \left(\frac{C_{dial}}{C_{ext}}\right) \times 100 \quad (1)$$

where C_{dial} is the CIP concentration in the microdialysate samples and C_{ext} is the CIP concentration in the medium surrounding the probe.

For the retrodialysis method, the probes ($n = 3$) were placed on a glass tube and immersed in blank Ringer's solution. Different CIP concentrations in Ringer's solution were pumped through the probes, and microdialysate samples were collected and analyzed by the LC fluorescence detection method. The relative recovery by retrodialysis (RR_{RD}; in percent) was calculated according to equation 2:

$$RR_{RD} = 100 - \left(\frac{C_{perf} - C_{dial}}{C_{perf}} \times 100\right) \quad (2)$$

where C_{dial} is CIP concentration in the microdialysate samples and C_{perf} is the drug concentration in the perfusate solution.

Animals. The animal experiments were approved by the Federal University of Rio Grande do Sul (UFRGS) Ethics in Animal Use Committee (protocol 24140). Six-week-old male Wistar rats (from the CREAL/UFRGS animal facility) were used for *P. aeruginosa* bead and blank bead inoculation. On the day of drug dosing, all animals (healthy and infected animals and animals inoculated with blank beads) were 8 weeks old and weighed between 250 and 300 g. The rats were maintained under controlled temperature and humidity with a 12-h light and 12-h dark cycle. Water and standard food were allowed *ad libitum* until the moment of the experiments.

Rat model of biofilm lung infection. The rat model of biofilm lung infection proposed by Johansen and Høiby (39) was used with minor modifications. The model is reported in the literature to produce a pulmonary infection that is stable for more than a month, and this chronic lung infection mimics what is found in human chronic lung infections, for example, infections in patients with cystic fibrosis (16, 17, 39–41). Briefly, *P. aeruginosa* cells were immobilized in spherical alginate beads to mimic the biofilm matrix effect and to prevent clearance from the lung after bacterial inoculation into the animals. For this purpose, 1 ml of the *P. aeruginosa* inoculum (10^9 CFU/ml) was mixed with 9 ml of a sterile alginate solution (11 mg/ml). The viscous suspension was sprayed by the use of compressed air into a cross-linking solution of 0.1 M $CaCl_2$ in Tris-HCl buffer (0.1 M, pH 7.0). The newly formed beads were cured for 1 h in the calcium bath with continuous stirring, after which they were centrifuged at 180 $\times$ *g* for 10 min and washed twice in sterile saline. Bead sizes were determined by Mastersizer analysis, and the final number of CFU was determined by plate dilutions. Since binding of CIP to alginate is not expected to occur (37), no studies of binding between CIP and alginate beads were conducted.

Six-week-old male Wistar rats were anesthetized (ketamine-xylazine, 100 and 10 mg/kg, respectively, intraperitoneally [i.p.]) and intratracheally challenged with 100 μl of the *P. aeruginosa* beads with the help of a MicroSprayer syringe (model IA-1B; Penn Century, Philadelphia, PA, USA). After the beads had been inoculated, the animals were allowed to recover from anesthesia with the head and body inclined slightly on a heated surface. The animals were maintained under standard conditions, and at 14 days after inoculation, CIP pharmacokinetics were investigated.

A study had earlier been conducted to determine the bacteriology in the lung after inoculation to ensure the development of infection. At 3, 5, 7, and 14 days after inoculation, the animals ($n = 3$ animals/day) were sacrificed, and the lungs were aseptically excised and homogenized with 5 ml of sterile saline. After the lung homogenates were serially diluted with sterile saline, 100-μl samples were plated on Mueller-Hinton agar and incubated at 37 $\pm$ 1°C (24 h), and the *P. aeruginosa* colonies were counted.

The lungs of infected rats and rats that received the blank beads were analyzed microscopically 14 days after inoculation ($n = 3$ animals/group). For the histopathological analysis, the tissues were fixed in a 10% neutral buffered formalin solution and embedded in paraffin blocks. The blocks were sliced and stained with eosin and hematoxylin dyes. The analyses were conducted by veterinary pathologists (Department of Veterinary Pathology, College of Veterinary, UFRGS, Porto Alegre, RS, Brazil).

Surgical procedure for probe insertion. For microdialysis probe insertion into the lung, the animals were anesthetized with urethane (1.25 g/kg i.p.) and immobilized in a supine position. After confirmation of anesthesia, the animals were intubated by tracheotomy and artificially ventilated using a rodent respirator (model 683; Harvard Apparatus, Holliston, MA, USA) at a frequency of 64 to 68 min^{-1} and with an air volume of 2.5 ml. The right lung was exposed through an open space between two ribs. The CMA/20 probe was inserted carefully into the intermediate lobe with the aid of a needle, which was removed after probe insertion. After probe insertion, the lung was thoroughly put back in place. Before the beginning of all experiments, a 1-h probe equilibration period with perfusion of Ringer's solution at a flow rate of 1.5 μl/min was performed. The surgical procedure for probe insertion used in this study is well described, and no major lung trauma induced by the microdialysis catheter has been reported in the literature (10, 11, 42, 43).

Microdialysis probe *in vivo* recovery. CIP microdialysis probe recovery *in vivo* was determined by retrodialysis (18). The animals were anesthetized with urethane (1.25 g/kg i.p.), and the CMA/20 probes were inserted into the lungs as described above. After a 1-h equilibration period, Ringer's solution was replaced by Ringer's solution containing CIP at 0.75 μg/ml, and five microdialysate samples of 45 μl each were collected at 30-min intervals. The *in vivo* recovery of CIP was calculated using equation 2. Because the probes were maintained under sink conditions throughout the experiments, the *in vivo* recovery of each probe was used to calculate the unbound CIP concentrations in each animal's lungs.

CIP lung penetration experimental design. To determine the CIP lung penetration, male Wistar rats were randomly divided into five groups ($n = 6$ animals/group): two healthy groups (one for blood sampling and one for lung microdialysate sampling), two *P. aeruginosa*-infected groups, and a control group inoculated with blank beads. The fifth group was added to the study to verify if the observed differences in the CIP lung free concentrations were due to the presence of alginate beads in the animals' lungs. All animals received CIP at 20 mg/kg by intravenous injection into the femoral vein.

For the microdialysis groups, the probes were inserted into the lung and Ringer's solution was pumped at a flow rate of 1.5 μl/min. The microdialysate samples were collected every 30 min up to 12 h after CIP administration. The unbound CIP concentrations in the lung were determined by correcting the measured microdialysate concentrations by the *in vivo* recovery.

For the plasma groups, the carotid artery was used for blood sampling. The animals were anesthetized with urethane (1.25 g/kg i.p.), and a cannula was surgically inserted into the artery. The cannula was maintained irrigated with heparinized saline (25 IU/ml). At predetermined times before (time zero) and

after (0.08, 0.25, 0.5, 1, 2, 4, 6, 8 and 12 h) i.v. bolus dosing, approximately 200 μl of blood was collected into heparinized tubes, and the plasma was immediately separated by centrifugation (12,000 rpm at 4 $\pm$ 1°C for 10 min). The plasma samples were stored at -80 ± 2°C for no more than 30 days before analysis (38).

Determination of plasma protein binding. The *in vitro* CIP binding to proteins in rat plasma was determined by microdialysis. Different CIP concentrations (0.3, 3, and 6 μg/ml) were used. The experiments were carried out with a pool of plasma from different animals. The *in vitro* probe recovery in plasma was determined by retrodialysis. The probe was inserted into an Eppendorf tube containing blank plasma, and CIP at 0.75 μg/ml in Ringer's solution was perfused at a flow rate of 1.5 μl/min. Microdialysate samples were collected every 30 min up to 2 h, and plasma recovery was calculated using equation 2.

For protein binding determination, blank plasma samples (990 μl) were spiked with 10 μl of the CIP solutions to result in the final total concentrations indicated above. An aliquot (100 μl) was separated for the determination of total plasma concentrations. Calibrated microdialysis probes ($n = 3$) were inserted in plasma samples and allowed to equilibrate at 37 $\pm$ 1°C for 1 h before sampling. Four samples were collected at 30-min intervals. The unbound concentrations were corrected by the *in vitro* probe recovery in plasma. Protein binding was determined as the ratio between the difference in the total and unbound concentrations and the total concentration.

Pharmacokinetic analysis. (i) NCA. Noncompartmental analysis (NCA) was used to determine the pharmacokinetic parameters in plasma and tissue. The plasma and lung concentration-versus-time profiles were analyzed individually for each animal using Phoenix software (Pharsight; Certara, USA). For the microdialysis data, the midpoint of the collection interval was used as the time set for NCA analysis, and the assayed concentration was hence assumed to reflect the concentration at that time point. CIP penetration into the lungs (*fT*) was determined as the ratio between the mean free lung tissue and the mean free plasma area under the concentration-time curve from time zero to infinity ($AUC_{0-\infty,tissue}/f_u \cdot AUC_{0-\infty,plasma}$), where f_u is the unbound fraction in rat plasma.

The PK parameters obtained by NCA for the healthy and infected animals and the blank bead-inoculated animals were compared by one-way analysis of variance (ANOVA) ($\alpha = 0.05$), followed by Tukey's test or Student's *t* test ($\alpha = 0.05$), as appropriate, employing SigmaStat (version 3.5) software (Systat Software, Point Richmond, CA, USA).

(ii) Population pharmacokinetic modeling. Experimental data were analyzed using the nonlinear mixed effect modeling approach in NONMEM (version 7.3; ICON Development Solutions, Ellicott City, MD, USA) (44). The first-order conditional estimation method with interaction (FOCE INTER) was applied in all estimations. The PsN (version 4.5.1) tool kit (45), the R (version 3.3.1) program (46), and the Xpose 4 (version 4.4.1) program (47) were used for automating and controlling the runs, data visualization, and graphical analysis (goodness-of-fit graphics, including visual predictive checks [VPCs]), respectively. The Pirana (version 2.9) program was used to keep track of run records and results.

A total of 526 observations (for 108 plasma samples and 418 lung microdialysate samples) from a total of 30 rats were included in the data set for the analysis. Data below the limit of quantification (BLOQ) were reported and kept in the data set since they represented less than 1% of the total data. Missing data were excluded from the analysis, no data for plasma were missing, and less than 5% of the data for microdialysate samples were missing.

The modeling was performed sequentially: first, a model for the plasma data was developed, and thereafter, microdialysis data were added and the model was expanded. In the final modeling step, parameters for both plasma and lung data were simultaneously estimated. Microdialysate samples were described by the integral over each collection interval (48) instead of a midpoint approach; therefore, no assumptions regarding collection times were made.

The effect of the covariate body weight (BW) on all parameters was investigated, and volume parameters were assumed to be directly proportional to BW (exponent of 1), while clearance parameters were raised to the power of 0.75 (49). Finally, the effects of infection and beads in all parameters were investigated with stepwise covariate modeling (SCM), using a forward inclusion process ($P < 0.05$) followed by backward elimination process ($P < 0.01$).

The confidence intervals for the parameters were obtained using the sampling importance resampling (SIR) procedure (50) implemented in PsN.

ACKNOWLEDGMENTS

Bruna G. S. Torres acknowledges the CAPES Foundation/Brazil for a Ph.D. scholarship and the PDSE Program (process 002416/2015-08). The National Council for Scientific and Technological Development (CNPq/Brazil) provided funding to Teresa Dalla Costa under grant number 480366/2012-8.

The funders had no role in study design, data collection and interpretation, or the decision to submit the work for publication.

We thank Luciana Sonne for performing the histological analysis.

B.G.S.T. participated in study design, animal experiments, analysis of the data, and writing of the article. V.E.H. and P.M.B. participated in study design and animal experiments. A.J.M. participated in study design, analysis of the data, and writing of the article. E.I.N. and L.E.F. participated in analysis of the data and writing of the article.

T.D.C. conceived the project, got funding, and participated in the study design, analysis of the data, and writing of the article.

REFERENCES

1. Strausbaugh SD, Davis PB. 2007. Cystic fibrosis: a review of epidemiology and pathobiology. Clin Chest Med 28:279–288. https://doi.org/10.1016/j.ccm.2007.02.011.
2. Kidd TJ, Ramsay KA, Vidmar S, Carlin JB, Bell SC, Wainwright CE, Grimwood K, ACFBAL Study Investigators. 2015. *Pseudomonas aeruginosa* genotypes acquired by children with cystic fibrosis by age 5-years. J Cyst Fibros 14:361–369. https://doi.org/10.1016/j.jcf.2014.12.007.
3. Macià MD, Perez JL, Molin S, Oliver A. 2011. Dynamics of mutator and antibiotic-resistant populations in a pharmacokinetic/pharmacodynamic model of Pseudomonas aeruginosa biofilm treatment. Antimicrob Agents Chemother 55:5230–5237. https://doi.org/10.1128/AAC.00617-11.
4. Ciofu O, Tolker-Nielsen T, Jensen PØ, Wang H, Høiby N. 2015. Antimicrobial resistance, respiratory tract infections and role of biofilms in lung infections in cystic fibrosis patients. Adv Drug Deliv Rev 85:7–23. https://doi.org/10.1016/j.addr.2014.11.017.
5. Burgess DS, Hall RG. 2007. Simulated comparison of the pharmacodynamics of ciprofloxacin and levofloxacin against *Pseudomonas aeruginosa* using pharmacokinetic data from healthy volunteers and 2002 minimum inhibitory concentration data. Clin Ther 29:1421–1427. https://doi.org/10.1016/j.clinthera.2007.07.024.
6. Hengzhuang W, Wu H, Ciofu O, Song Z, Høiby N. 2011. Pharmacokinetics/pharmacodynamics of colistin and imipenem on mucoid and nonmucoid *Pseudomonas aeruginosa* biofilms. Antimicrob Agents Chemother 55:4469–4474. https://doi.org/10.1128/AAC.00126-11.
7. Hengzhuang W, Wu H, Ciofu O, Song Z, Høiby N. 2012. *In vivo* pharmacokinetics/pharmacodynamics of colistin and imipenem in *Pseudomonas aeruginosa* biofilm infection. Antimicrob Agents Chemother 56:2683–2690. https://doi.org/10.1128/AAC.06486-11.
8. Hengzhuang W, Ciofu O, Yang L, Wu H, Song Z, Oliver A, Høiby N. 2013. High β-lactamase levels change the pharmacodynamics of β-lactam antibiotics in *Pseudomonas aeruginosa* biofilms. Antimicrob Agents Chemother 57:196–204. https://doi.org/10.1128/AAC.01393-12.
9. Hammarlund-Udenaes M. 2006. Microdialysis for characterization of PK/PD relationships, p 589–600. *In* Handbook of behavioral neuroscience, vol 16. Elsevier Academic Press, San Diego, CA. https://doi.org/10.1016/S1569-7339(06)16031-2.
10. Zimmermann ES, Laureano JV, Dos Santos CN, Schmidt S, Lagishetty CV, De Castro WV, Dalla Costa T. 2016. Simultaneous semimechanistic population analyses of levofloxacin in plasma, lung, and prostate to describe the influence of efflux transporters on drug distribution following intravenous and intratracheal administration. Antimicrob Agents Chemother 60:946–954. https://doi.org/10.1128/AAC.02317-15.
11. Dhanani J, Roberts JA, Chew M, Lipman J, Boots RJ, Paterson DL, Fraser JF. 2010. Antimicrobial chemotherapy and lung microdialysis: a review. Int J Antimicrob Agents 36:491–500. https://doi.org/10.1016/j.ijantimicag.2010.08.013.
12. Marchand S, Dahyot C, Lamarche I, Mimoz O, Couet W. 2005. Microdialysis study of imipenem distribution in skeletal muscle and lung extracellular fluids of noninfected rats. Antimicrob Agents Chemother 49:2356–2361. https://doi.org/10.1128/AAC.49.6.2356-2361.2005.
13. Dahyot C, Marchand S, Pessini GL, Pariat C, Debaene B, Couet W, Mimoz O. 2006. Microdialysis study of imipenem distribution in skeletal muscle and lung extracellular fluids of *Acinetobacter baumannii*-infected rats. Antimicrob Agents Chemother 50:2265–2267. https://doi.org/10.1128/AAC.00190-06.
14. Crandon JL, Kim A, Nicolau DP. 2009. Comparison of tigecycline penetration into the epithelial lining fluid of infected and uninfected murine lungs. Antimicrob Agents Chemother 64:837–839. https://doi.org/10.1093/jac/dkp301.
15. Kuti JL, Nicolau DP. 2015. Presence of infection influences the epithelial lining fluid penetration of oral levofloxacin in adult patients. Int J Antimicrob Agents 45:512–518. https://doi.org/10.1016/j.ijantimicag.2014.12.028.
16. Growcott EJ, Coulthard A, Amison R, Hardaker EL, Saxena V, Malt L, Jones P, Grevot A, Poll C, Osborne C, Banner KH. 2011. Characterisation of a refined rat model of respiratory infection with *Pseudomonas aeruginosa* and the effect of ciprofloxacin. J Cyst Fibros 10:166–174. https://doi.org/10.1016/j.jcf.2010.12.007.
17. Yan P, Chen Y, Song Z, Wu H, Kong J, Qin X. 2008. Pathogenic effects of biofilm with chronic *Pseudomonas aeruginosa* lung infection in rats. J Nanjing Med Univ 22:34–38. https://doi.org/10.1016/S1007-4376(08)60007-6.
18. de Lange ECM, de Boer AG, Breimer DD. 2000. Methodological issues in microdialysis sampling for pharmacokinetic studies. Adv Drug Deliv Rev 45:125–148. https://doi.org/10.1016/S0169-409X(00)00107-1.
19. Hurtado FK, Weber B, Derendorf H, Hochhaus G, Dalla Costa T. 2014. Population pharmacokinetic modeling of the unbound levofloxacin concentrations in rat plasma and prostate tissue measured by microdialysis. Antimicrob Agents Chemother 58:678–686. https://doi.org/10.1128/AAC.01884-13.
20. Boxenbaum H. 1982. Interspecies scaling, allometry, physiological time, and the ground plan of pharmacokinetics. J Pharmacokinet Biopharm 10:201–227. https://doi.org/10.1007/BF01062336.
21. Sweet CS, Emmert SE, Seymour AA, Stabilito II, Oppenheimer L. 1987. Measurement of cardiac output in anesthetized rats by dye dilution using a fiberoptic catheter. J Pharmacol Methods 17:189–203. https://doi.org/10.1016/0160-5402(87)90050-7.
22. De Araujo BV, Diniz A, Palma EC, Buffé C, Dalla Costa T. 2011. PK-PD modeling of β-lactam antibiotics: *in vitro* or *in vivo* models? J Antibiot (Tokyo) 64:439–446. https://doi.org/10.1038/ja.2011.29.
23. Gonzalez D, Schmidt S, Derendorf H. 2013. Importance of relating efficacy measures to unbound drug concentrations for anti-infective agents. Clin Microbiol Rev 26:274–288. https://doi.org/10.1128/CMR.00092-12.
24. Gaohua L, Wedagedera J, Small BG, Almond L, Romero K, Hermann D, Hanna D, Jamei M, Gardner I. 2015. Development of a multicompartment permeability-limited lung PBPK model and its application in predicting pulmonary pharmacokinetics of antituberculosis drugs. CPT Pharmacometrics Syst Pharmacol 4:605–613. https://doi.org/10.1002/psp4.12034.
25. Reisfeld B, Metzler CP, Lyons MA, Mayeno AN, Brooks EJ, Degroote MA. 2012. A physiologically based pharmacokinetic model for capreomycin. Antimicrob Agents Chemother 56:926–934. https://doi.org/10.1128/AAC.05180-11.
26. Zhu L, Zhang Y, Yang J, Wang Y, Zhang J, Zhao Y, Dong W. 2016. Prediction of the pharmacokinetics and tissue distribution of levofloxacin in humans based on an extrapolated PBPK model. Eur J Drug Metab Pharmacokinet 41:395–402. https://doi.org/10.1007/s13318-015-0271-8.
27. Morgan ET. 2009. Impact of infectious and inflammatory disease on cytochrome P450-mediated drug metabolism and pharmacokinetics. Clin Pharmacol Ther 85:434–438. https://doi.org/10.1038/clpt.2008.302.
28. LeBel M, Bergeron MG, Vallée F, Fiset C, Chassé G, Bigonesse P, Rivard G. 1986. Pharmacokinetics and pharmacodynamics of ciprofloxacin in cystic fibrosis patients. Antimicrob Agents Chemother 30:260–266. https://doi.org/10.1128/AAC.30.2.260.
29. Vance-Bryan K, Guay D, Rotschafer J. 1990. Clinical pharmacokinetics of ciprofloxacin. Clin Pharmacokinet 19:434–461. https://doi.org/10.2165/00003088-199019060-00003.
30. Gontijo AV, Brillault J, Grégoire N, Lamarche I, Gobin P, Couet W, Marchand S. 2014. Biopharmaceutical characterization of nebulized antimicrobial agents in rats. 1. Ciprofloxacin, moxifloxacin, and grepafloxacin. Antimicrob Agents Chemother 58:3942–3949. https://doi.org/10.1128/AAC.02818-14.
31. Dan M, Torossian K, Weissberg D, Kitzes R. 1993. The penetration of ciprofloxacin into bronchial mucosa, lung parenchyma, and pleural tissue after intravenous administration. Eur J Clin Pharmacol 44:101–102. https://doi.org/10.1007/BF00315290.
32. Brunner M, Hollenstein U, Delacher S, Jäger D, Schmid R, Lackner E, Georgopoulos A, Eichler HG, Müller M. 1999. Distribution and antimicrobial activity of ciprofloxacin in human soft tissues. Antimicrob Agents Chemother 43:1307–1309.
33. Cheng PW, Boat TF, Shaikh S, Wang OL, Hu PC, Costa DL. 1995. Differential

effects of ozone on lung epithelial lining fluid volume and protein content. Exp Lung Res 21:351–365. https://doi.org/10.3109/01902149509023713.
34. Kiem S, Schentag JJ. 2008. Interpretation of antibiotic concentration ratios measured in epithelial lining fluid. Antimicrob Agents Chemother 52:24–36. https://doi.org/10.1128/AAC.00133-06.
35. Davies D. 2003. Understanding biofilm resistance to antibacterial agents. Nat Rev Drug Discov 2:114–122. https://doi.org/10.1038/nrd1008.
36. Tseng BS, Zhang W, Harrison JJ, Quach TP, Song JL, Penterman J, Singh PK, Chopp DL, Packman AI, Parsek MR. 2013. The extracellular matrix protects *Pseudomonas aeruginosa* biofilm by limiting the penetration of tobramycin. Environ Microbiol 15:2865–2878. https://doi.org/10.1111/1462-2920.12155.
37. Abdi-Ali A, Mohammadi-Mehr M, Agha Alaei Y. 2006. Bactericidal activity of various antibiotics against biofilm-producing *Pseudomonas aeruginosa*. Int J Antimicrob Agents 27:196–200. https://doi.org/10.1016/j.ijantimicag.2005.10.007.
38. Zimmermann E, Torres BG, Dalla Costa T. 2016. Validation of a sensitive HPLC/fluorescence method for assessment of ciprofloxacin levels in plasma and prostate microdialysate samples from rats. Biomed Chromatogr 30:330–336. https://doi.org/10.1002/bmc.3552.
39. Johansen HK, Høiby N. 1999. Rat model of chronic *Pseudomonas aeruginosa* lung infection, p 517–529. *In* Zak O, Sande MA (ed), Handbook of animal models of infection: experimental models in antimicrobial chemotherapy. Elsevier Academic Press, San Diego, CA.
40. Bragonzi A. 2010. Murine models of acute and chronic lung infection with cystic fibrosis pathogens. Int J Med Microbiol 300:584–593. https://doi.org/10.1016/j.ijmm.2010.08.012.
41. van Heeckeren AM, Schluchter MD. 2002. Murine models of chronic Pseudomonas aeruginosa lung infection. Lab Anim 36:291–312. https://doi.org/10.1258/002367702320162405.
42. Tasso L, Bettoni CC, Oliveira LK, Dalla Costa T. 2008. Evaluation of gatifloxacin penetration into skeletal muscle and lung by microdialysis in rats. Int J Pharm 358:96–101. https://doi.org/10.1016/j.ijpharm.2008.02.023.
43. Li Y, Wang Z, Xiao H, Ning Y, Zhou J, Liu R, Huang Y. 2016. A microdialysis study of pharmacokinetics of orally or intravenously administrated levofloxacin in lung tissues of the Streptococcus pneumoniae pneumonia rat. Int J Clin Exp Med 9:7247–7255.
44. Beal S, Sheiner LB, Boeckmann A, Bauer RJ. 2009. NONMEM users guides (1989-2009). ICON Development Solutions, Ellicott City, MD.
45. Lindbom L, Pihlgren P, Jonsson EN. 2005. PsN-toolkit—a collection of computer intensive statistical methods for non-linear mixed effect modeling using NONMEM. Comput Methods Programs Biomed 79:241–257. https://doi.org/10.1016/j.cmpb.2005.04.005.
46. R Core Team. 2012. R: a language and environment for statistical computing. R Foundation for Statistical Computing, Vienna, Austria.
47. Jonsson EN, Karlsson MO. 1999. Xpose—an S-PLUS based population pharmacokinetic/pharmacodynamic model building aid for NONMEM. Comput Methods Programs Biomed 58:51–64.
48. Tunblad K, Hammarlund-Udenaes M, Jonsson EN. 2004. An integrated model for the analysis of pharmacokinetic data from microdialysis experiments. Pharm Res 21:1698–1707. https://doi.org/10.1023/B:PHAM.0000041468.00587.c6.
49. Holford NH. 1996. A size standard for pharmacokinetics. Clin Pharmacokinet 30:329–332. https://doi.org/10.2165/00003088-199630050-00001.
50. Dosne AG, Bergstrand M, Harling K, Karlsson MO. 2016. Improving the estimation of parameter uncertainty distributions in nonlinear mixed effects models using sampling importance resampling. J Pharmacokinet Pharmacodyn 43:583–596. https://doi.org/10.1007/s10928-016-9487-8.